



PAPER

Two-photon absorption in quantum dots with Hellmann potential

RECEIVED
28 January 2024REVISED
19 April 2024ACCEPTED FOR PUBLICATION
14 May 2024PUBLISHED
24 May 2024Nguyen N Hieu^{1,2} , Le Dinh³, N A Poklonski⁴ , Ha Phan Thi Hai⁵ and Huynh V Phuc^{6,*} ¹ Institute of Research and Development, Duy Tan University, Da Nang 550000, Vietnam² Faculty of Natural Sciences, Duy Tan University, Da Nang 550000, Vietnam³ Center for Theoretical and Computational Physics, University of Education, Hue University, Hue 530000, Vietnam⁴ Faculty of Physics, Belarusian State University, Minsk 220030, Belarus⁵ Faculty of Medicine, Nguyen Tat Thanh University, Ho Chi Minh City 700000, Vietnam⁶ Division of Physics, School of Education, Dong Thap University, Cao Lanh 870000, Vietnam

* Author to whom any correspondence should be addressed.

E-mail: hieunn@duytan.edu.vn and hvphuc@dthu.edu.vn**Keywords:** two-photon absorption, spherical quantum dot, Hellmann potential**Abstract**

We study the nonlinear optical absorption properties of a spherical quantum dot (SQD) with Hellmann potential, focusing on the two-photon absorption (TPA) process, using GaAs/AlGaAs material as an example. The radial Schrödinger equation is solved using the Nikiforov-Uvarov method, while the two-photon absorption coefficient is determined through second-order perturbation theory concerning the electron-photon interaction. Our study shows that the intraband transition has a smaller energy transition than the interband transition, leading to TPA spectra for the intraband transition that is restricted within a smaller energy range and exhibits a higher peak value than those for the interband transition. The peak corresponding to the orbital quantum number of electrons in SQD $\ell = 2$ consistently appears to the left of the peak corresponding to $\ell = 1$ in both intraband and interband transition cases. Additionally, the dependence of the absorption peak position on the order of transition, n , differs between intra- and inter-band transitions. We also observe blue shift behavior in the TPA spectra as all three parameters, r_0 , V_{0e} , and η , increase. Our investigation has the potential to enable the design of novel photonic devices, ultra-fast optical switches, and highly efficient solar cells through the optimization of quantum dot material properties.

The linear and nonlinear optical absorption properties of low-dimensional systems (LDSs), such as quantum wells [1–4], quantum dots [5–7], nanowires [8–10], and nanotubes [11, 12], have received significant attention due to their potential for practical applications in photonics, optoelectronics, and quantum computing. Quantum confinement effects, a unique aspect of LDSs, can greatly modify the electronic and optical properties of materials [13]. Among of these LDSs, quantum dots, including spherical quantum dots (SQDs), exhibit optical properties depending on their size, attributed to quantum confinement [14]. As the dimensions of quantum dots reduce, the bandgap increases, resulting in a blue shift in absorption and emission spectra. Additionally, quantum dots feature broad absorption spectra, enabling light absorption across a wide range [6]. Conversely, they emit light at a notably narrow wavelength, determined by their size. This characteristic proves advantageous in applications like LEDs and photovoltaics, where efficient light absorption and emission are paramount. Consequently, numerous researchers have undertaken extensive investigations into QD systems [15–18].

Since quantum dots exhibit discrete energy levels and quantization of the energy spectrum as a result of strong electron confinement, the two-photon absorption (TPA) spectra of quantum dots are expected to be significantly different from those of bulk materials. Moreover, the TPA process in LDSs is strongly influenced by the size and shape of the nanoscale materials and the carrier dynamics [19–21]. The confinement potential governs the spatial distribution of electronic states, which also affects the TPA process. The theoretical and experimental study of nonlinear optical absorption properties of LDSs has led to the development of novel optoelectronic and photonic devices [22, 23], including ultra-fast optical switches [24], optical modulators

[25, 26], and photodetectors [27, 28]. The study of nonlinear optical absorption in LDSs remains an active area of research with a promising future for applications in various fields.

The Hellmann potential, which was first presented by Hellmann [29, 30], is a combination of the Coulomb and the Yukawa potentials [31]. Compared to these individual potentials, the Hellmann potential has the advantage of allowing more accurate modeling of the behavior of charged particles at short and long distances. Therefore, the properties of this potential type have caught the attention of numerous researchers [32–35]. Dutt *et al.* [32] used the shifted large- N expansion method to analyze the bound states of the Hellmann potential. Their study showed that the method can still be applied to the screened Coulomb potential with reasonably accurate results, which may have practical applications in calculating atomic processes. Roy *et al.* [33] used a generalized pseudospectral method to calculate the bound states of the Hellmann potential. They obtained energy eigenvalues and densities with high accuracy by using a nonuniform, optimal spatial discretization of the radial Schrödinger equation. The results include ground and excited states for various potential parameters and stronger couplings. In another work, Hamzavi *et al.* [34] used the generalized parametric Nikiforov-Uvarov (NU) method [36, 37] to find solutions for the radial Schrödinger equation (SE) of the Hellmann potential. Their work presents closed-form calculations for the eigenvalues and eigenfunctions, as well as numerical results that agree well with other methods. Furthermore, the paper includes energy levels of the pure Coulomb potential as a specific case. The use of the supersymmetric approach to solve the Schrödinger equation with the Hellmann potential is also discussed in the study [35]. The centrifugal term is approximated and the solutions for other potentials, including the Coulomb potential and Yukawa potential, are derived by transforming variables from the Hellmann potential.

The theory of two-photon absorption coefficient was recently developed by Gong *et al.* [21] associated with both interband transitions and intraband transitions under the second-order perturbation theory with respect to the electron-photon interaction [19, 20]. This theory was then successfully applied to investigate the TPA properties of quantum rings [38]. In this study, we investigate the nonlinear optical properties of a GaAs/AlGaAs SQD with the Hellmann potential by studying the two-photon absorption (TPA) process. We present in detail the wave function and energy of the electron confined in the SQD, using the NU method [34, 36, 37] to find the solution of the radial Schrödinger equation. The expression for the TPA coefficient is derived through the transition matrix element, including both intra and interband transition processes. We show the TPA spectra as a function of photon energy for different quantum states. Additionally, we study in detail the effect of the adjustable parameter r_0 , potential depth V_{0e} , and potential parameter η on the TPA spectra.

1. Model and analytical results

1.1. Solution of radial Schrödinger equation

We consider a SQD subjected to the Hellmann potential. The Hellmann potential is defined as follows [29–35]

$$V(r) = -\frac{A}{r} - \frac{Be^{-\epsilon r}}{r}, \quad (1)$$

where $\epsilon = 1/r_0$ is an adjustable parameter. The terms A and B characterize the strength of Hellmann potential, which are related to potential depth V_{0i} ($i = e/h$ for the electron/hole) and the parameter r_0 as $A = V_{0i}r_0$ and $B = \eta V_{0i}r_0$, with η being a parameter. Here, we followed the approach outlined in previous studies [6, 39, 40] to define the parameters A and B . The SE for an electron confined in a SQD can be expressed as follows

$$\left[-\frac{\hbar^2}{2m^*} \nabla^2 + V(r) \right] \psi_{n\ell m}(r, \theta, \phi) = E_{n\ell} \psi(r, \theta, \phi), \quad (2)$$

where m^* is the effective mass of electron and ∇^2 is the Laplacian in spherical coordinates. Using the wave function in the form

$$\psi_{n\ell m}(r, \theta, \phi) = R_{n\ell}(r) Y_{\ell m}(\theta, \phi) = \frac{G_{n\ell}(r)}{r} Y_{\ell m}(\theta, \phi), \quad (3)$$

with $Y_{\ell m}(\theta, \phi)$ being the spherical harmonic functions, we get the following equation for the radial wave function

$$\frac{d^2 G_{n\ell}(r)}{dr^2} + \frac{2m^*}{\hbar^2} [E_{n\ell} - V_{\text{eff}}(r)] G_{n\ell}(r) = 0, \quad (4)$$

where the effective potential is

$$V_{\text{eff}}(r) = V(r) + \frac{\lambda}{r^2}, \quad (5)$$

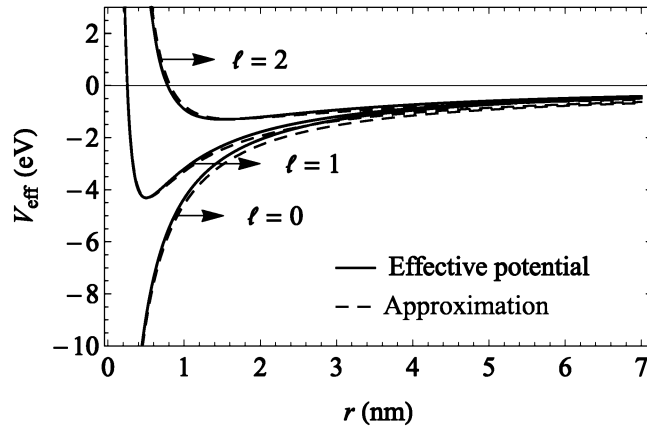


Figure 1. The effective potential, V_{eff} in equation (5) and its approximation in equation (7) for different values of ℓ . The results are calculated for GaAs/AlGaAs SQD with $m_e^* = 0.067m_0$, $V_{0e} = 228 \text{ meV}$, $r_0 = 10 \text{ nm}$, and $\eta = 1$.

with $\lambda = \hbar^2 \ell(\ell + 1)/2m^*$. Since equation (4) cannot be solved analytically, we use the following approximation for the centrifugal term as [41–43]

$$\frac{1}{r} \approx \frac{\epsilon}{1 - e^{-\epsilon r}}. \quad (6)$$

Hence, the effective potential in equation (5) becomes

$$V_{\text{eff}}(r) \approx -\frac{A\epsilon}{1 - e^{-\epsilon r}} - \frac{B\epsilon e^{-\epsilon r}}{1 - e^{-\epsilon r}} + \frac{\lambda\epsilon^2}{(1 - e^{-\epsilon r})^2}. \quad (7)$$

We can see from figure 1 that the approximation shown in equation (6) works quite good. Substituting equation (7) into equation (4) and then making the transformation $\xi = e^{-\epsilon r}$ we get

$$\left[\frac{d^2}{d\xi^2} + \frac{1}{\xi} \frac{d}{d\xi} + \frac{-a_1\xi^2 + a_2\xi - a_3}{\xi^2(1 - \xi)^2} \right] G_{n\ell}(\xi) = 0, \quad (8)$$

where

$$a_1 = \frac{2m^*B}{\epsilon\hbar^2} + \frac{\mathcal{E}}{\epsilon^2}, \quad \mathcal{E} = -\frac{2m^*E_{n\ell}}{\hbar^2}, \quad (9)$$

$$a_2 = \frac{2\mathcal{E}}{\epsilon^2} - \frac{2m^*}{\epsilon\hbar^2}(A - B), \quad (10)$$

$$a_3 = \frac{\mathcal{E}}{\epsilon^2} - \frac{2m^*A}{\epsilon\hbar^2} + \frac{2m^*\lambda}{\hbar^2}. \quad (11)$$

Applying the NU method [34, 36, 37], we obtain the following solutions to equation (8) as

$$G_{n\ell}(\xi) = N_{n\ell} \xi^{\lambda_1} (1 - \xi)^{\lambda_2} P_n^{(2\lambda_1, 2\lambda_2-1)}(1 - 2\xi), \quad (12)$$

where $\lambda_1 = \sqrt{a_3}$, $\lambda_2 = \ell + 1$, $P_n^{(\mu, \nu)}(\xi)$ are the Jacobi polynomials, and $N_{n\ell}$ is normalization constant, which is found from the normalization condition

$$1 = \int_0^\infty |R_{n\ell}(r)|^2 r^2 dr = \int_0^1 |G_{n\ell}(r)|^2 dr. \quad (13)$$

Using a coordinate transformation $t = 1 - 2\xi$, we have

$$1 = \frac{N_{n\ell}^2}{2\epsilon} \int_{-1}^1 \left(\frac{1-t}{2} \right)^{2\lambda_1-1} \left(\frac{1+t}{2} \right)^{2\lambda_2} [P_n^{(2\lambda_1, 2\lambda_2-1)}(t)]^2 dt. \quad (14)$$

We use the integral of the form (see Appendix A)

$$\begin{aligned} & \int_{-1}^1 \left(\frac{1-t}{2} \right)^{2\lambda_1-1} \left(\frac{1+t}{2} \right)^{2\lambda_2} [P_n^{(2\lambda_1, 2\lambda_2-1)}(t)]^2 dt \\ &= 2\Gamma(2\lambda_2 + 1) \left[\frac{(2\lambda_1 + 1)_n}{n!} \right]^2 J_0(n, \lambda_1, \lambda_2), \end{aligned} \quad (15)$$

where $(n)_k$ is the Pochhammer symbol, and

$$J_0(n, \lambda_1, \lambda_2) = \sum_{k=0}^n \frac{(-n)_k (a_{0n})_k \Gamma(b_0)}{k! (c_0)_k \Gamma(d_0)} {}_3F_2(-n, a_{0n}, b_0; c_0, d_0; 1). \quad (16)$$

Here, we have denoted $a_{0n} = n + 2(\lambda_1 + \lambda_2)$, $b_0 = 2\lambda_1 + k$, $c_0 = 2\lambda_1 + 1$, and $d_0 = 2\lambda_1 + 2\lambda_2 + k + 1$. The normalization constant is found as

$$N_{n\ell} = \frac{n!}{(2\lambda_1 + 1)_n} \sqrt{\frac{\epsilon}{\Gamma(2\lambda_2 + 1) J_0(n, \lambda_1, \lambda_2)}}, \quad (17)$$

which did not show in the previous work [34]. The corresponding energy levels, obtained from the NU method [34, 36, 37], are

$$E_{n\ell} = -\frac{\epsilon^2 \hbar^2}{2m^*} \left[C^2 + \frac{2m^* A}{\epsilon \hbar^2} - \ell(\ell + 1) \right], \quad (18)$$

$$C = \frac{2m^*(A + B)/\epsilon \hbar^2 - (n + \ell + 1)^2 - \ell(\ell + 1)}{2(n + \ell + 1)}, \quad (19)$$

under the condition

$$(n + \ell + 1)^2 + \ell(\ell + 1) \leq \frac{2m^*}{\epsilon \hbar^2} (A + B). \quad (20)$$

The condition in equation (20) reveals that the number of states in SQD with Hellmann potential is finite.

The effective potential and probability density of the radial wave-function, $|R_{n\ell}(r)|^2 r^2$, for the first few states are shown in figure 2(a)-(c). As r increases, V_{eff} tends to approach zero. For $\ell = 0$, V_{eff} increases monotonically and has no left barrier, while for $\ell \neq 0$ states, the effective potential displays a left barrier. The depth and width of the potential decrease and increase, respectively, as ℓ increases. The probability density of locating a particle based on radius is illustrated by the dashed lines. The peaks signify positions where the probability of finding a particle is highest. It is observable that the quantity of peaks is proportional to the quantum number n . For every quantum number n , there exist $n + 1$ positions where the probability of finding a particle is maximal. Note that the shape, depth, and width of the potential are determined by the values of $V_{0\ell}$, r_0 , and ℓ , which significantly affect the TPA spectra.

1.2. Two-photon absorption coefficient

Two-photon absorption (TPA) is a nonlinear optical process in which two photons are simultaneously absorbed by an electron confined in the systems, resulting in the excitation of the system to a higher energy state. In contrast to the conventional one-photon absorption, TPA requires the simultaneous absorption of two photons to occur. When a quantum system is excited by an incident light of energy $\hbar\omega$ and magnitude $I_0 = 2c\epsilon_0 n_r \omega^2 A_0^2$ [44] (c is the speed of light, n_r is the refractive index of the material, ϵ_0 is the vacuum permittivity, and A_0 is the amplitude of the vector potential for the light field), the absorption coefficient due to the two-photon process is calculated using the following expression [19–21]:

$$K_2 = \frac{8\pi\omega}{\Omega I_0^2} \sum_{i,f} |\mathcal{M}_{if}|^2 \delta(E_f - E_i - 2\hbar\omega). \quad (21)$$

In equation (21), Ω is the normalized volume of the system, the sum is taken over all possible initial, $|i\rangle$, and final, $|f\rangle$, states, and the transition matrix element is expressed as follows

$$\mathcal{M}_{if} = \sum_{\zeta} \frac{\langle f | \mathcal{H}_I | \zeta \rangle \langle \zeta | \mathcal{H}_I | i \rangle}{E_{\zeta} - E_i - \hbar\omega - i\hbar\gamma_{\zeta}}. \quad (22)$$

Here, the subscript ζ and γ_{ζ} denote the intermediate virtual state and its inverse lifetime, respectively. In equation (22), \mathcal{H}_I is the electron-photon interaction which is expressed in the form [21]

$$\mathcal{H}_I = -\frac{e}{m^*} \mathbf{A}_p \cdot \mathbf{p}, \quad (23)$$

where $\mathbf{A}_p = A_0(\mathbf{e}_r + e^{\pm i\pi/2} \mathbf{e}_{\phi})/\sqrt{2}$ is the light vector potential with \pm stands for right and left polarization, respectively [45], and $\mathbf{p} = -i\hbar\nabla$ is the electron momentum operator. Using equation (23), we obtain the following result for the matrix element for the transition between two states $|\zeta_0\rangle = |n_0, \ell_0, m_0\rangle$ and $|\zeta_1\rangle = |n_1, \ell_1, m_1\rangle$

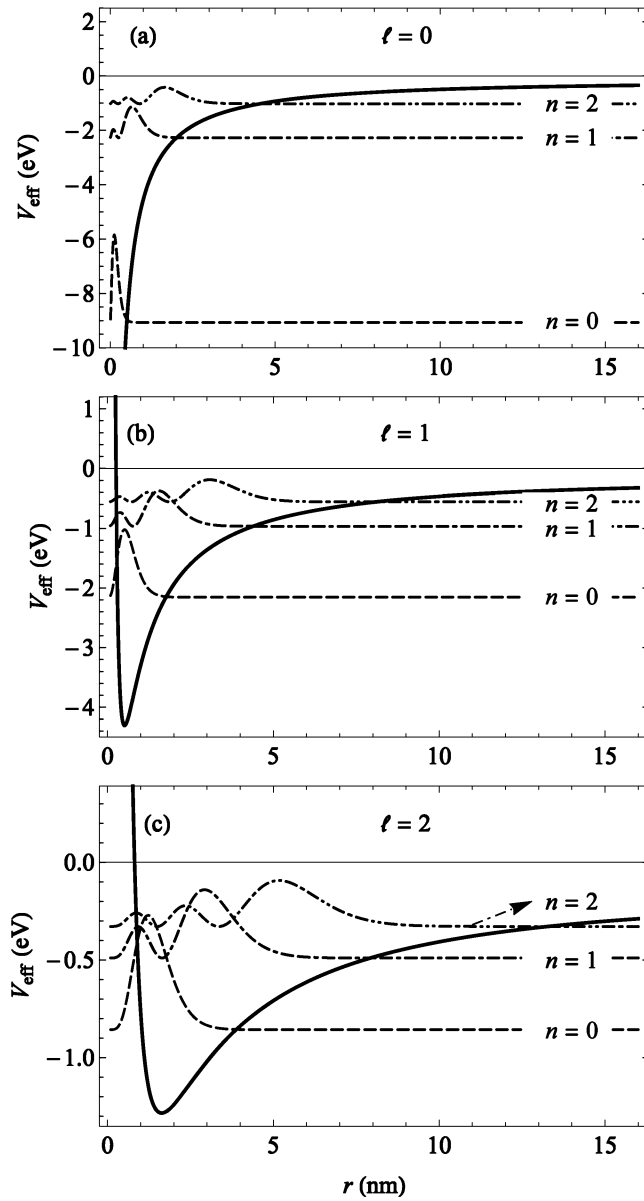


Figure 2. The effective potential (blue solid curves) and the probability densities for various states: (a) $\ell = 0$, (b) $\ell = 1$, and (c) $\ell = 2$. The input parameters are the same as in figure 1.

$$\langle \varsigma_1 | \mathcal{H}_1 | \varsigma_0 \rangle = -\frac{i e \omega A_0}{\epsilon \sqrt{2}} \delta_{\ell_0, \ell_1} \delta_{m_0, m_1} (2\lambda_2 + 1) \frac{J_0(n_0, n_1, \lambda_1, \lambda_2)}{\sqrt{J_0(n_0, \lambda_1, \lambda_2) J_0(n_1, \lambda_1, \lambda_2)}}, \quad (24)$$

where

$$J_0(n_0, n_1, \lambda_1, \lambda_2) = \sum_{k=0}^{n_0} \frac{(-n_0)_k (a_{0n_0})_k \Gamma(b_0)}{k! (c_0)_k \Gamma(d_0)} {}_3F_2(-n_1, a_{0n_1}, b_0; c_0, d_0; 1), \quad (25)$$

with $a_{0n_i} = n_i + 2(\lambda_1 + \lambda_2)$, the same with that appears below equation (16). Delta functions in equation (24) confirm the selection rules that transitions only occur between states with identical quantum numbers ℓ and m .

2. Results and discussion

In this section, we report our results on the TPA coefficient in GaAs/AlGaAs SQD. The following input parameters are used [46–48]: $m_e^* = 0.067m_0$ ($m_h^* = 0.079m_0/0.45m_0$) is the electron (light/heavy hole) effective mass, where m_0 is the free electron mass, $E_g = 1.607$ eV is the energy gap, $n_r = 3.2$, and $V_{0h} = 0.67V_{0e}$. The delta-function in equation (21) is approximated by the Lorentzian with $\hbar\gamma = \hbar\gamma_v = 10$ meV.

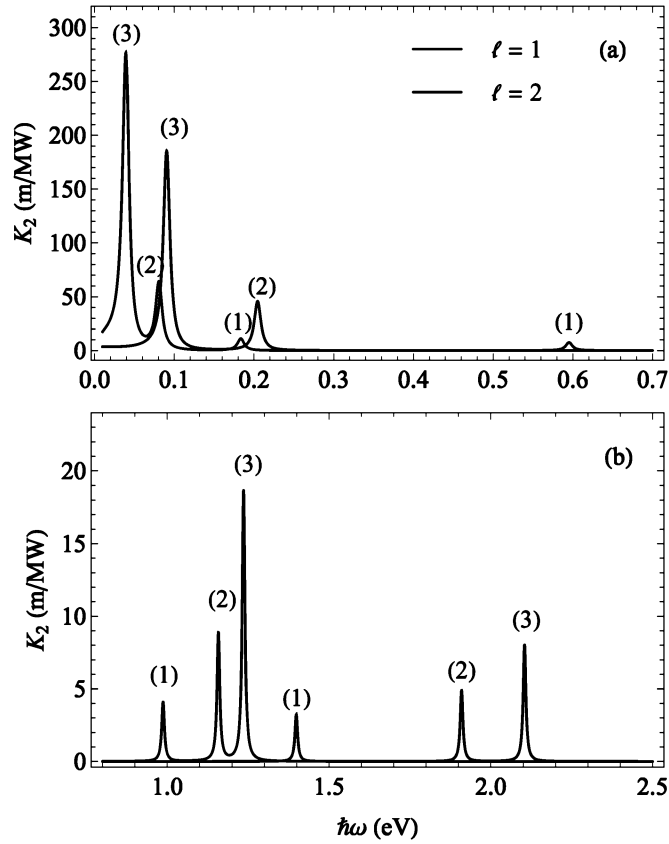


Figure 3. (a) Intra-conduction band and (b) interband transitions TPA spectra at $V_{0e} = 228$ meV, $r_0 = 10$ nm, and $\eta = 1$. Explanations for the labels (1), (2), and (3) see in the text.

We present the TPA spectra as a function of photon energy for two values of ℓ in figure 3. The labels (1), (2), and (3) in both intra-conduction band and interband transitions correspond to the transition $n \rightarrow n + 1$ with $n=0,1$, and 2, respectively. The peak positions of the TPA spectra, which represents the absorbed photon energy, is equal to the energy transition $\Delta E_{n'\ell',n\ell} = E_{n'\ell'} - E_{n\ell}$, or equivalently, $2\hbar\omega$. Additionally, the peak value of the TPA spectra is inversely proportional to the energy transition. We observe that the intraband transition has a smaller energy transition compared to the interband transition. As a result, the TPA spectra for the intraband transition (figure 3(a)) are localized in a smaller energy range and have a larger peak value compared to the TPA spectra for the interband transition (figure 3(b)), similar to that in quantum ring [38]. On the other hand, from figure 2, we can see that as ℓ increases, the distance between energy levels decreases. In other words, $\Delta E_{n'\ell',n\ell}$ is inversely proportional to ℓ . Therefore, the position of the peak corresponding to $\ell = 2$ is always to the left of the peak corresponding to $\ell = 1$ in both intraband and interband transition cases. On the other hand, the dependence of the absorption peak position on the order of transition, n , for intra- and inter-band transitions is different. For the intraband transition case, as shown in figure 3(a), as the order of transition increases, the position of the absorption peak shifts towards the low-energy region. This is a result of the fact that $\Delta E_{n'\ell',n\ell}^{\text{intra}}$ decreases as n increases. In contrast, for interband transitions, as shown in figure 3(b), since $\Delta E_{n'\ell',n\ell}^{\text{inter}}$ increases with n , the position of the absorption peak shifts towards the high-energy region as the order of the transition increases. Specifically, the peaks corresponding to the transitions $|1, 1\rangle \rightarrow |2, 1\rangle$ and $|2, 1\rangle \rightarrow |3, 1\rangle$ (marked as peaks labeled red (2) and (3) in figure 3(b)) reside within the visible light spectrum. This indicates the potential utilization of quantum dots characterized by the parameters outlined in figure 3 for the production of LEDs emitting light within the visible region.

In figure 4, we show the TPA spectra for the $|0, 1\rangle \rightarrow |1, 1\rangle$ transition as a function of photon energy for three different values of r_0 . It should be noted that here we only illustrate the transition $|0, 1\rangle \rightarrow |1, 1\rangle$, but it is still valid for other cases. We can see that, in both intra- and inter-band transition cases, as r_0 increases, the position of the absorption peak shifts towards the high-energy region (blue-shifts), and at the same time, the height of the absorption peak decreases. This blue-shift behavior reveals that as the value of r_0 increases, the shifting energy $\Delta E_{01,11}^{\text{intra}}/2$ also increases, which is evident in the inset.

Figure 5 shows the TPA spectra as a function of photon energy for three different values of $V_{0e} = 0.8V_0$, V_0 , and $1.2V_0$, where $V_0 = 228$ meV. The figure shows that as V_{0e} increases, the absorption peak undergoes a blue

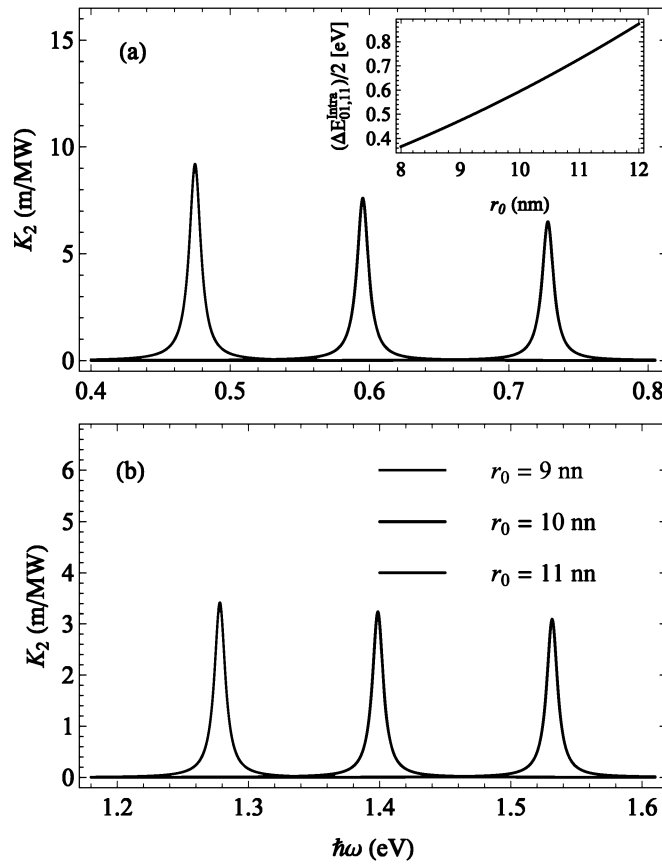


Figure 4. (a) Intra-conduction band and (b) interband transitions TPA spectra for the $n = 0 \rightarrow n = 1$ transition with $\ell = 1$. The results are calculated for different values of r_0 at $V_{0e} = 228$ meV and $\eta = 1$. The inset shows the $\Delta E_{01,1}^{\text{intra}}/2$ in the units of eV.

shift for both intra- and inter-band transition cases. This is because $\Delta E_{01,1}^{\text{intra}}/2$ increases as V_{0e} increases, as shown in the inset. Physically, this implies that as the potential depth increases, the energy of the absorbed photon also increases.

Figure 6 depicts the TPA spectra as a function of photon energy for three distinct values of η . When $\eta = 0$, the Hellmann potential reduces to the Coulomb potential, causing the absorption peak to appear at the lowest energy. When η rises, both intra- and inter-band transitions exhibit a blue shift in the absorption peak as a result of the increase in $\Delta E_{01,1}^{\text{intra}}/2$ with η , as displayed in the inset.

3. Conclusions

We investigated the nonlinear optical absorption properties of a SQD with Hellmann potential by analyzing the two-photon absorption process, with the GaAs/AlGaAs material serving as an example. Our numerical findings indicate that the intraband transition has a smaller energy transition compared to the interband transition. Thus, the TPA spectra for the intraband transition are restricted within a smaller energy range and exhibit a higher peak value than the TPA spectra for the interband transition. In both intraband and interband transition cases, the position of the peak corresponding to $\ell = 2$ is consistently to the left of the peak corresponding to $\ell = 1$. Furthermore, the dependence of the absorption peak position on the order of transition, n , differs between intra- and inter-band transitions. The TPA spectra exhibit blue shift behavior as any of the parameters, r_0 , V_{0e} , or η , increases.

To summarize, our investigation into the nonlinear optical absorption properties of quantum dots with Hellmann potential offers numerous opportunities for practical application in optoelectronics. By optimizing the quantum dot material properties, it may be possible to design novel photonic devices, ultra-fast optical switches, and highly efficient solar cells.

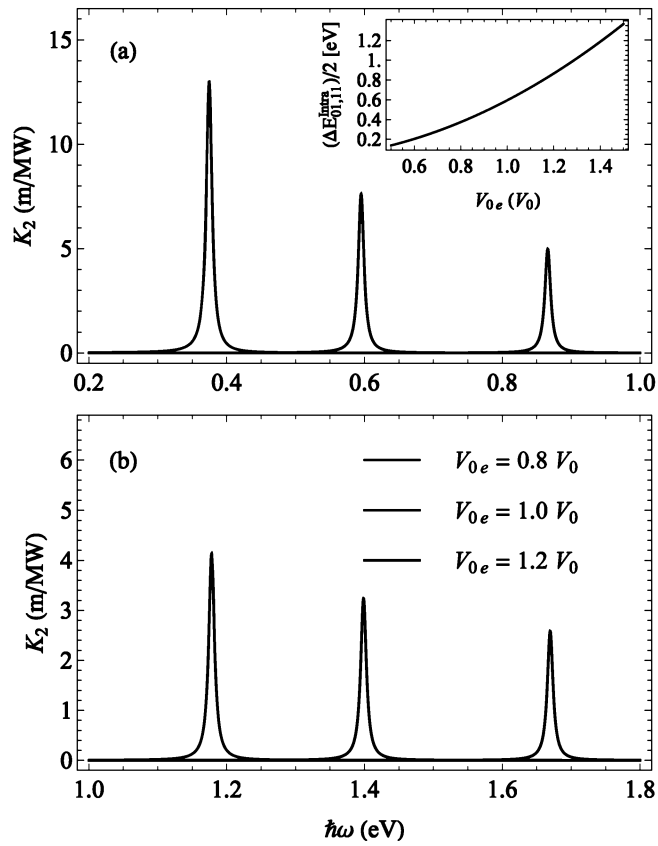


Figure 5. (a) Intra-conduction band and (b) interband transitions TPA spectra for the $n = 0 \rightarrow n = 1$ transition with $\ell = 1$. The results are calculated for different values of V_{0e} (with $V_0 = 228$ meV) at $r_0 = 10$ nm and $\eta = 1$. The inset shows the $\Delta E_{01,11}^{\text{intra}}/2$ in the units of eV.

Acknowledgments

N. A. Poklonski acknowledges the support from the Belarusian Republican Foundation for Fundamental Research (Grant No. F23RNF-049) and the Belarusian National Research Program ‘Convergence-2025’.

Data availability statement

All data that support the findings of this study are included within the article (and any supplementary files).

Appendix A. An integral for Jacobi polynomials

We consider an integral of the form

$$I = \int_{-1}^1 \left(\frac{1-x}{2} \right)^\alpha \left(\frac{1+x}{2} \right)^\beta P_n^{(\mu,\nu)}(x) P_m^{(\delta,\gamma)}(x) dx. \quad (\text{A.1})$$

The Jacobi polynomials are expressed in terms of hypergeometric function as [49, 50]

$$\begin{aligned} P_n^{(\mu,\nu)}(x) &= \binom{n+\mu}{n} {}_2F_1 \left(-n, n+\mu+\nu+1; \mu+1; \nu+1; \frac{1-x}{2} \right) \\ &= \binom{n+\mu}{n} \sum_{k=0}^n \frac{(-n)_k (n+\mu+\nu+1)_k}{k! (\mu+1)_k} \left(\frac{1-x}{2} \right)^k. \end{aligned} \quad (\text{A.2})$$

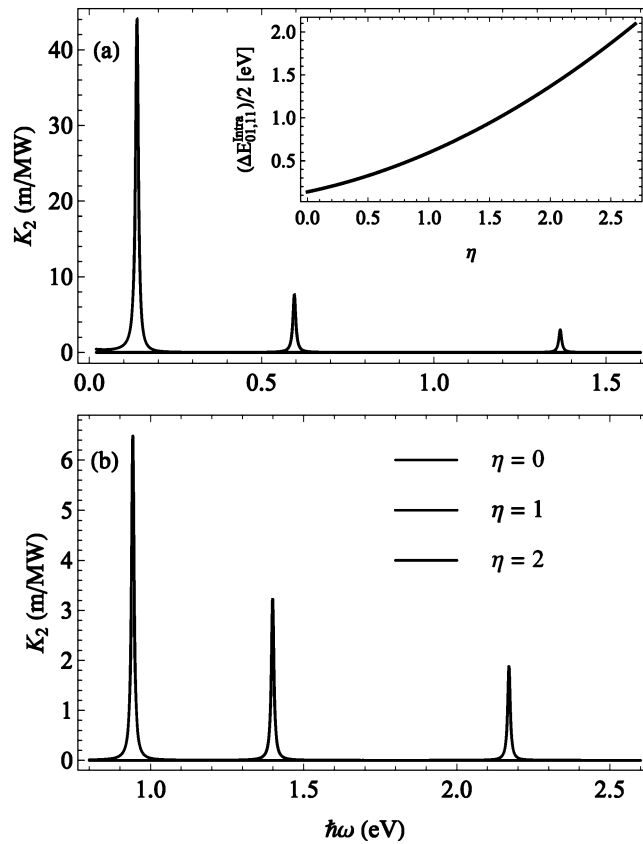


Figure 6. (a) Intra-conduction band and (b) interband transitions TPA spectra for the $n = 0 \rightarrow n = 1$ transition with $\ell = 1$. The results are calculated for different values of η at $r_0 = 10$ nm and $V_{0e} = 228$ meV. The inset shows the $\Delta E_{01,11}^{\text{intra}}/2$ in the units of eV.

Using equation (A.2), equation (A.1) becomes

$$I = \frac{(\mu + 1)_n}{n!} \frac{(\delta + 1)_m}{m!} \sum_{k=0}^n \frac{(-n)_k (n + \mu + \nu + 1)_k}{k! (\mu + 1)_k} \times \sum_{\ell=0}^m \frac{(-m)_\ell (m + \delta + \gamma + 1)_\ell}{\ell! (\delta + 1)_\ell} \int_{-1}^1 \left(\frac{1-x}{2} \right)^{\alpha+k+\ell} \left(\frac{1+x}{2} \right)^\beta dx. \quad (\text{A.3})$$

We use the standard integral that, for $k > -1, \ell > -1$ [49]

$$\int_{-1}^1 \left(\frac{1-t}{2} \right)^k \left(\frac{1+t}{2} \right)^\ell dt = \frac{2\Gamma(k+1)\Gamma(\ell+1)}{\Gamma(k+\ell+2)}. \quad (\text{A.4})$$

equation (A.3) becomes

$$I = 2\Gamma(\beta + 1) \frac{(\mu + 1)_n}{n!} \frac{(\delta + 1)_m}{m!} \times \sum_{k=0}^n \frac{(-n)_k (n + \mu + \nu + 1)_k \Gamma(\alpha + k + 1)}{k! (\mu + 1)_k \Gamma(\alpha + \beta + k + 2)} \times \sum_{\ell=0}^m \frac{(-m)_\ell (m + \delta + \gamma + 1)_\ell (\alpha + k + 1)_\ell}{\ell! (\delta + 1)_\ell (\alpha + \beta + k + 2)_\ell}. \quad (\text{A.5})$$

The summation over ℓ in equation (A.5) can be replaced by the generalized hypergeometric function. The equation (A.5) now becomes

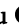
$$I = 2\Gamma(\beta + 1) \frac{(\mu + 1)_n}{n!} \frac{(\delta + 1)_m}{m!} J(n, m, \alpha, \beta, \mu, \nu, \gamma, \delta), \quad (\text{A.6})$$

where


$$J(n, m, \alpha, \beta, \mu, \nu, \delta, \gamma) = \sum_{k=0}^n \frac{(-n)_k (a_{n,\mu,\nu})_k \Gamma(b)}{k! (c_\mu)_k \Gamma(d)} {}_3F_2(-m, a_{m,\delta,\gamma}, b; c_\delta, d; 1).$$

Here, we have denoted $a_{n,\mu,\nu} = n + \mu + \nu + 1$, $b = \alpha + k + 1$, $c_\mu = \mu + 1$, and $d = \alpha + \beta + k + 2$. Substituting $n=m$, $\alpha = 2\lambda_1 - 1$, $\beta = 2\lambda_2$, $\mu = \delta = 2\lambda_1$, and $\nu = \gamma = 2\lambda_2 - 1$ into equation (A.6) and making some simple calculations, we will get the standard result shown in equation (15) of the main text.

ORCID iDs

Nguyen N Hieu  <https://orcid.org/0000-0001-5721-960X>

N A Poklonski  <https://orcid.org/0000-0002-0799-6950>

Huynh V Phuc  <https://orcid.org/0000-0001-8063-0923>

References

- [1] Zhao Q, Aqiqi S, You J F, Kria M, Guo K X, Feddi E, Zhang Z H and Yuan J H 2020 *Physica E* **115** 113707
- [2] Tung L V, Vinh P T and Phuc H V 2018 *Physica B* **539** 117
- [3] Phuc H V and Van Tung L 2014 *Superlattices Microstruct.* **71** 124
- [4] Nasa S and Purohit S P 2020 *Physica E* **118** 113913
- [5] Sargsian T A, Mkrtchyan M A, Sarkisyan H A and Hayrapetyan D B 2021 *Physica E* **126** 114440
- [6] Máthé L, Onyenegecha C P, Farcaş A A, Pioraş-Ţimbolmaş L M, Solaimani M and Hassanabadi H 2021 *Phys. Lett. A* **397** 127262
- [7] Gieseke R L M 2019 *Chem. Mater.* **31** 6850
- [8] Ben-Zvi R, Bar-Elli O, Oron D and Joselevich E 2021 *Nat. Commun.* **12** 3286
- [9] Liu J, Nie H, Yan B, Yang K, Yang H, Khayrudinov V, Lipsanen H, Zhang B and He J 2020 *Photon. Res.* **8** 1035
- [10] Khudiyakov D V, Lobach A S and Nadtchenko V A 2009 *Appl. Opt.* **48** 1624
- [11] Guo G Y, Chu K C, Wang D S and Duan C G 2004 *Phys. Rev. B* **69** 205416
- [12] Zorman B, Ramakrishna M V and Friesner R A 1995 *J. Phys. Chem.* **99** 7649
- [13] Rezaei G, Mousazadeh Z and Vaseghi B 2010 *Physica E* **42** 1477
- [14] Dakhlaoui H, Belhadj W, Musa M O and Ungan F 2023 *Optik* **277** 170684
- [15] Khordad R and Mirhosseini B 2014 *Opt. Spectrosc.* **117** 434
- [16] Chang C, Li X, Wang X and Zhang C 2023 *Phys. Lett. A* **467** 128732
- [17] Mese A I, Cicek E, Ozkapi S G, Ozkapi B and Erdogan I 2024 *Phys. Status Solidi B* **260** 2300133
- [18] Nathan V, Guenther A H and Mitra S S 1985 *J. Opt. Soc. Am. B* **2** 294
- [19] Fedorov A V, Baranov A V and Inoue K 1996 *Phys. Rev. B* **54** 8627
- [20] Gong R, Zhou C and Feng X 2022 *Phys. Rev. B* **105** 195301
- [21] Wu J J, Tao Y R, Wu X C and Chun Y 2017 *J. Alloys Compd.* **713** 38
- [22] Liu J *et al* 2019 *J. Phys. Chem. Lett.* **10** 4429
- [23] Seo S B, Nah S, Sajjad M, Singh N, Shin Y, Kim Y, Kim J and Sim S 2022 *Phys. Rev. Appl.* **18** 014010
- [24] Liu J, Li X, Feng J, Zheng C, Wang Y, Wang A and Liu X 2020 *Ann. Phys.* **532** 1900454
- [25] Chen F 2018 *Micro Nano Lett.* **13** 758
- [26] Lv Z, Liu L, Zhangyang X, Sun Y, Lu F and Tian J 2021 *Opt. Commun.* **486** 126799
- [27] Lv Z, Liu L, Zhangyang X, Sun Y, Lu F and Tian J 2021 *Physica E* **126** 114496
- [28] Hellmann H 1935 *J. Chem. Phys.* **3** 61
- [29] Hellmann H and Kassatotschkin W 1936 *J. Chem. Phys.* **4** 324
- [30] Adamowski J 1985 *Phys. Rev. A* **31** 43
- [31] Dutt R, Mukherji U and Varshni Y P 1986 *Phys. Rev. A* **34** 777
- [32] Roy A K, Jalbout A F and Proynov E I 2008 *J. Math. Chem.* **44** 260
- [33] Hamzavi M, Thylwe K E and Rajabi A A 2013 *Commun. Theor. Phys.* **60** 1
- [34] Onate C A, Onyeaju M C, Ikot A N and Ebomwonyi O 2017 *Eur. Phys. J. Plus* **132** 462
- [35] Nikiforov A F and Uvarov V B 1988 *Special Functions of Mathematical Physics: A Unified Introduction with Applications* 1st ed (Birkhäuser Boston, MA)
- [36] Tezcan C and Sever R 2009 *Int. J. Theor. Phys.* **48** 337
- [37] Phuc H V 2023 *J. Appl. Phys.* **133** 074303
- [38] Li X, Duan Y and Ma Y 2022 *Commun. Theor. Phys.* **74** 085702
- [39] Li X and Chang C 2022 *Opt. Materials* **131** 112605
- [40] Hamzavi M, Movahedi M, Thylwe K E and Rajabi A A 2012 *Chin. Phys. Lett.* **29** 080302
- [41] Hamzavi M, Ikhdair S M and Thylwe K E 2013 *J. Math. Chem.* **51** 227
- [42] Greene R L and Aldrich C 1976 *Phys. Rev. A* **14** 2363
- [43] Chuang S L 2012 *Physics of Photonic Devices* 2nd ed (New York: Wiley)
- [44] Catarina G, Have J, Fernández-Rossier J and Peres N M R 2019 *Phys. Rev. B* **99** 125405
- [45] Bastard G 1990 *Wave mechanics Applied to Semiconductor Heterostructures* (New York: Wiley)
- [46] Aghoutane N, El-Yadri M, El-Aouami A, Feddi E, Dujardin F, El-Haouari M, Duque C A, Nguyen C V and Phuc H V 2019 *Appl. Phys.* **125** 17
- [47] Li E H 2000 *Physica E* **5** 215
- [48] Erdélyi A (ed) 1954 *Tables of Integral Transforms* Vol 2 (New York: McGraw-Hill)
- [49] Arora M S and Bajpai S D 1995 *Demonstr. Math.* **28** 177
- [50] Phuc H V 2015 *J. Phys. Chem. Solids* **82** 36